Development of a broadband nonlinear two-degree-of-freedom piezoelectric energy harvester

Wu, Hao; Soh, Chee Kiong; Tang, Lihua; Yang, Yaowen

2014

Development of a broadband nonlinear two-degree-of-freedom piezoelectric energy harvester

Hao Wu[1], Lihua Tang[1,2], Yaowen Yang[1]*, Chee Kiong Soh[1]

[1] Nanyang Technological University, 50 Nanyang Avenue, Singapore 639798

[2] Department of Mechanical Engineering, University of Auckland, 20 Symonds Street, Auckland 1010, New Zealand

* Corresponding author, yyw@pmail.ntu.edu.sg

ABSTRACT

Vibration energy harvesting using piezoelectric material has received great research interest in the recent years. One important concern for the development of piezoelectric energy harvesting is to broaden the operating bandwidth. Various techniques have been proposed for broadband energy harvesting, such as the resonance tuning approach, the frequency up-conversion technique, the multi-modal harvesting and the nonlinear technique. A recently reported linear 2-degree-of-freedom harvester can achieve two close resonant frequencies both with significant power outputs, using its unique cantilever configuration. This paper proposes to incorporate magnetic nonlinearity into the linear 2-DOF system, aiming at further broadening its operating bandwidth. Experimental parametric study is carried out to investigate the behavior of such nonlinear 2-DOF harvester. Among different configurations, an optimal configuration of the nonlinear 2-DOF harvester is obtained to achieve significantly wider bandwidth. A lumped parameter model for such nonlinear 2-DOF harvester is developed, and the results provide good validation for the experimental findings.

Keywords: piezoelectric; energy harvesting; broadband; multi-modal; nonlinear

1. INTRODUCTION

To power the small electronics such as wireless sensor, a promising alternative for chemical batteries is the use of energy harvesters, which harness ambient environmental energy and convert it into electricity. There are different possible energy resources for harvesting, including solar, wind, thermal

and vibration. Among them, mechanical vibration is the most ubiquitous energy source in our daily life, thus vibration based energy harvesting has attracted great research interest in recent years.

Generally, vibration energy can be converted into electrical energy using electrostatic, electromagnetic or piezoelectric effects. No matter what kind of mechanism is adopted, harvesters are mostly designed as a resonator providing large amplitude response within a quite narrow bandwidth. With a slight frequency shift from the resonance, the performance will decrease drastically. To improve the functionality of a vibration energy harvester, broadening the operation bandwidth is an important issue, as the vibration sources in the practical circumstances are usually frequency-variant or cover a large frequency range.

To achieve broadband energy harvesting, multi-modal technique as one promising method has been widely investigated, can be divided into two different themes according to their configurations. A system comprising an array of cantilever beams with different resonant frequencies can achieve wider bandwidth covered by all cantilever harvester components (Shahruz, 2006; Ferrari et al. 2008). However, such system sacrifices the overall output efficiency, as only one component is at work while others are off-resonance. Lien and Shu (2012) also studied the electrical behaviors for piezoelectric energy harvester arrays with different circuit interfaces. Another way for multi-modal energy harvesting is using more than one vibration modes based on a single cantilever beam. Energy harvester with conventional cantilever configuration can also provide multiple resonances; however, its high-order vibration modes are usually separated very far away from the fundamental one with much smaller amplitude (Ou et al., 2012; Tang et al., 2012; Erturk et al., 2009b). To design a multi-modal energy harvester which is more applicable, its multiple response peaks should be tuned close enough. Jang et al. (2011) and Kim et al. (2011) developed energy harvesting devices using both translational and rotational vibration motions to achieve two close resonant frequencies. Wu et al. (2013) proposed a "cut-out" 2-degree-of-freedom (2-DOF) harvester with a secondary beam enclosed within the main beam, which achieves two close resonances with significantly large amplitudes. Besides, this design can fully utilize the material of a cantilever beam.

Other than the multi-modal energy harvesting technique, magnetic interaction is frequently employed for broadband energy harvesting. Initially, the magnetic interaction is used to adjust the system stiffness and tune the resonant frequency to match the environmental excitation (Tang et al., 2013; Challa et al., 2008). But the magnet induced nonlinearity can also significantly change the behavior

thus performance of the harvester. Such harvesters are thus termed nonlinear energy harvesters. In general, most proposed nonlinear harvesters can be regarded as a Duffing-type oscillator developed from a linear single-degree-of-freedom (SDOF) harvester. They can be operated either in mono-stable or bi-stable condition depending on its configuration (Stanton et al., 2009; Cottone et al., 2009; Tang et al., 2012; Erturk et al., 2009a). Different oscillation states co-exist within same frequency range, such as high-amplitude oscillations, low-amplitude oscillations or chaotic vibrations. In the mono-stable configuration, its frequency response curve will cover a larger frequency range by "deflecting" the peak toward higher frequency or lower frequency direction. For bi-stable configuration, large amplitude vibration can be achieved when the base excitation is large enough to ensure the harvester to overcome the potential barrier between the two equilibrium positions. For the bi-stable harvesters developed by Erturk et al. (2009a), remarkable improvement is achieved under sufficient excitation (e.g. 0.35g), while no obvious improvement is reported for lower excitation level.

In this paper, a nonlinear 2-DOF piezoelectric energy harvester (PEH) is proposed based on the linear 2-DOF harvester developed by the authors (Wu et al., 2013). Experimental parametric study is carried out and a significantly broader operating bandwidth is achieved in mono-stable condition. A lumped parameter model for such nonlinear 2-DOF harvester is derived and the results present consistent trends compared to the experiment data. Based on the findings from experiment and modeling, it is concluded that, such nonlinear 2-DOF configuration is much more advantageous than linear 2-DOF configuration, by combining the multi-modal energy harvesting with nonlinear technique.

2. PREVIOUS LINEAR 2-DOF PIEZOELECTRIC ENERGY HARVESTER

A 2-DOF "cut-out" PEH was reported in our previous study (Wu et al., 2013), which achieves two close natural frequencies, and both the main beam (outer beam) and secondary beam (inner beam) can generate significant power outputs. The drawback of this linear 2-DOF PEH is the existence of an anti-resonance frequency. The response at the anti-resonance frequency will be very low and even approach zero when the damping in the system is very small. The presence of the anti-resonance in-between the two response peaks results in a deep valley in the response, which definitely deteriorates the broadband performance of the 2-DOF system. To further study the anti-resonance response as well as the entire frequency response of such 2-DOF harvester, a simplified "cut-out" beam shown Figure 1 is analyzed, which can be represented as a 2-DOF lumped mass model. In this model, the outer beam (two identical

arms) and inner beam are both assumed uniform, with L_1 and L_2 being the length of the outer beam and inner beam, respectively, and M_1 and M_2 the masses at the tips of outer beam and inner beam, respectively.

For the lumped mass model of this 2-DOF beam, the mass matrix is

$$[M] = \begin{bmatrix} M_1 & 0 \\ 0 & M_2 \end{bmatrix} \tag{1}$$

The stiffness matrix can be obtained as follows by using the standard stiffness influence coefficients method (Meirovitch 2003),

$$[K] = \frac{6EI_1}{4EI_1L_1^3L_2^3 + 3EI_2L_1^4L_2^2} \begin{bmatrix} 2EI_1L_2^3 + 2EI_2L_1^3 + 6EI_2L_1L_2^2 - 6EI_2L_1^2L_2 & -2EI_2L_1^3 + 3EI_2L_1^2L_2 \\ -2EI_2L_1^3 + 3EI_2L_1^2L_2 & 2EI_2L_1^3 \end{bmatrix} \tag{2}$$

where E is the elastic modulus of the material, and I_1 and I_2 are the moment of inertias of the outer and inner beams, respectively. Thus, the two resonant frequencies as well as the modal shapes can be obtained by solving the eigenvalue problem from the equation of motion for such 2-DOF system.

By solving the equation of motion for the 2-DOF system under base excitation, its frequency response can be obtained. The frequency response curves can be classified into different groups according to the values of L_1/L_2 and two natural frequencies f_1 and f_2, as shown in Table 1. Here the two natural frequencies f_1 and f_2 are not defined by the order of the absolute value of the frequency. Instead, f_1 denotes the natural mode in which the movement of the outer mass dominates, while f_2 relates to the inner mass. The mode shapes corresponding to f_1 and f_2 are also illustrated in Figure 1.
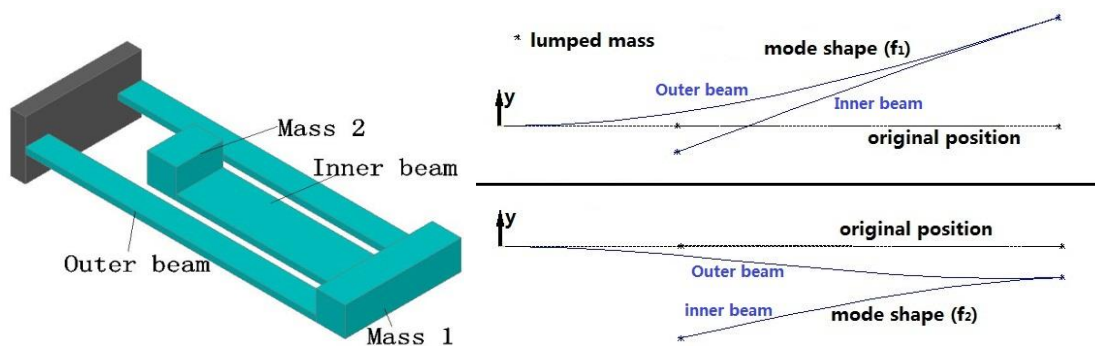

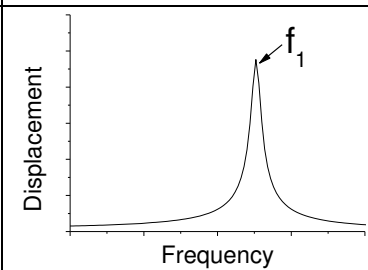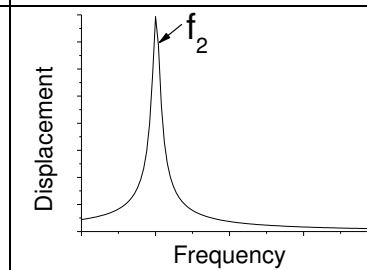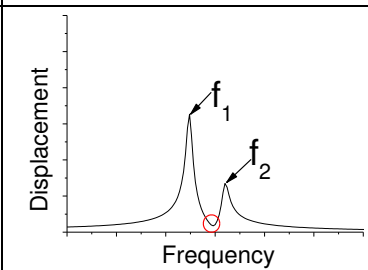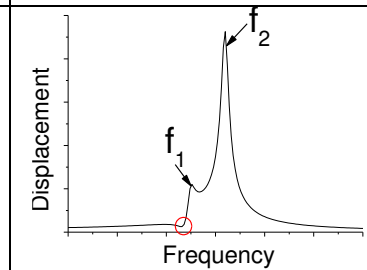Figure 1. A "cut-out" 2-DOF cantilever beam, and its mode shapes in lumped mass model

First of all, this table shows that, the frequency responses of the 2-DOF beam greatly rely on the length ratio of the inner beam to outer beam, while the value of 2/3 is a critical point that divides the pattern into three categories.
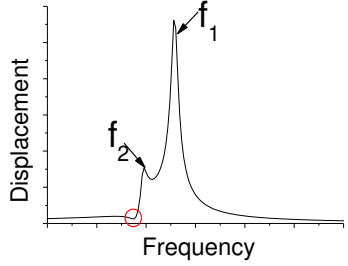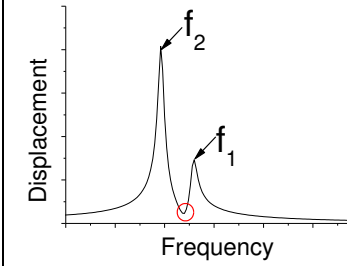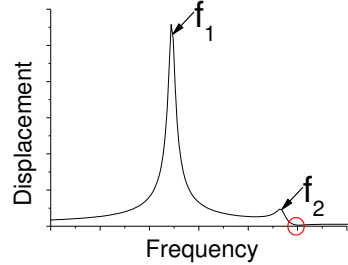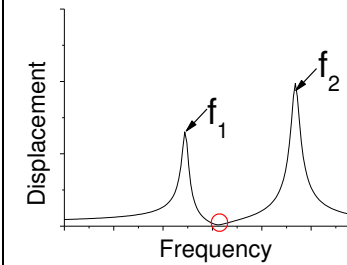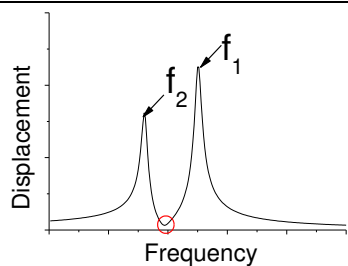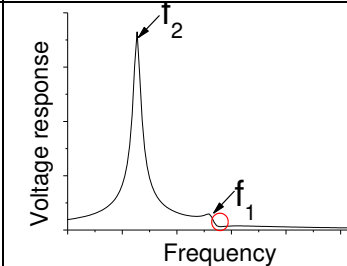
4

From Equation (2), it can be seen that when the length ratio L_2/L_1 equals to 2/3, the stiffness matrix will be reduced into a diagonal matrix, which fully decomposes the system to be two SDOF systems. This can also be observed from Group A in Table 1, i.e., the response curves are the same as the two independent SDOF systems.

If the length ratio L_2/L_1 is larger than 2/3, the system will follow the response pattern in Group B or C. As shown in group B, when $f_2 > f_1$, there is an anti-resonance point (highlighted with a red circle) in-between the two response peaks for the outer beam. This anti-resonance separates the two peaks and forms a deep valley in the response curve. The outer beam will not be able to generate sufficient power output around this valley due to the low response. The existence of anti-resonance between the two peaks will greatly deteriorate the performance of the harvester. There is an anti-resonance point for the inner beam as well, with its position in front of the two response peaks. In this condition, the valley in-between the two response peaks is not deep, and the inner beam can still generate significant power output throughout this frequency region.

By adjusting the values of the moment of inertia and the tip masses, natural frequency f_2 for the vibration mode dominated by the inner mass can be tuned lower than f_1, as represented by Group C in Table 1. By comparing Groups B and C, it can be observed that the response patterns for the outer beam and inner beam is swapped.

Table 1. Frequency response patterns

L_2/L_1	f_2/f_1	Displacement frequency response for outer mass M_1	Displacement frequency response for inner mass M_2	Remark
=2/3				Group A
>2/3	>1			Group B

	<1	f_2 f_1 (Displacement vs Frequency)	f_2 f_1 (Displacement vs Frequency)	Group C
<2/3	>1	f_1 f_2 (Displacement vs Frequency)	f_1 f_2 (Displacement vs Frequency)	Group D
	<1	f_2 f_1 (Displacement vs Frequency)	f_2 f_1 (Voltage response vs Frequency)	Group E

In Groups D and E with the length ratio smaller than 2/3, for $f_2 > f_1$, the anti-resonance point is located at the right of the two response peaks for the outer beam, while the inner beam has the anti-resonance response <mark>in-between</mark> the two peaks. Moreover, it also observed from Groups D and E, when the order of the natural frequencies exchanges, the patterns of the response curve swaps.

As conclude from Table 1, to design such a linear "cut-out" 2-DOF broadband energy harvester, one may prefer to have its frequency response with two close significant peaks, but without the anti-resonance <mark>in-between</mark> them (i.e. the response from the inner beam in Group B in Table 1).

3. EXPERIMENTAL STUDY OF THE NONLINEAR 2-DOF HARVESTER

<mark>3.1 Design of nonlinear 2-DOF harvester</mark>

Based on the design of the linear 2-DOF "cut-out" harvester, the nonlinear 2-DOF harvester is developed by introducing magnetic interaction. It comprises a main beam (outer beam) and a secondary beam (inner beam), both with tip masses. Two polar opposite magnets are installed at the tip of the

6

inner beam and the base, respectively. Figure 2 shows the prototype installed on a vertical seismic shaker.
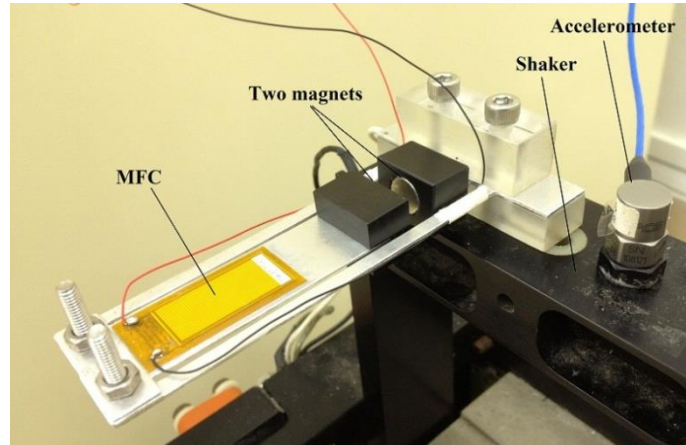

Figure 2. Nonlinear 2-DOF energy harvester installed on the vertical shaker

As discussed in Section 2, except for Group A in Table 1, an anti-resonance valley always exists in the frequency responses of both the outer and inner beams, but at different locations. Thus, only one beam (either outer beam or inner beam) can avoid the anti-resonance in-between the two response peaks for broadening bandwidth. In this experimental study, the inner beam is selected and optimized for further broadband energy harvesting by avoiding anti-resonance in-between two peaks and introducing nonlinearity. One d_{31} piezoelectric sheet, Macro-Fiber-Composite (MFC, model: M-2814-P2), is attached on the inner beam for energy generation. Two repulsive NdFeB permanent magnets with diameter of 10 mm, thickness of 5 mm and surface flux of 3500 gauss are embedded in two plastic holders, separated at the distance of D. One holder with the magnet serves as the tip mass of the inner beam (M_2=7.4 g), while the other one is clamped to the shaker with a short support beam. The length of the short support beam is adjustable, making it convenient to adjust the distance between the two magnets while keeping other structural parameters unchanged. The outer and inner beams have the thickness of 1 mm and 0.6 mm, respectively, both of which are made of aluminum. For the convenience of fabrication, these two parts are fabricated separately and assembled with screws. The screws and several pieces of steel plate at the free end of the outer beam serve as its tip mass (M_1), and M_1 is adjustable by adding or removing small steel plates. Each piece of small plate weighs about 1.9 g, while the minimum value of M_1 including the screws and nuts is 3.6 g. Detailed dimensions of the proposed nonlinear 2-DOF harvester are shown in Figure 3.
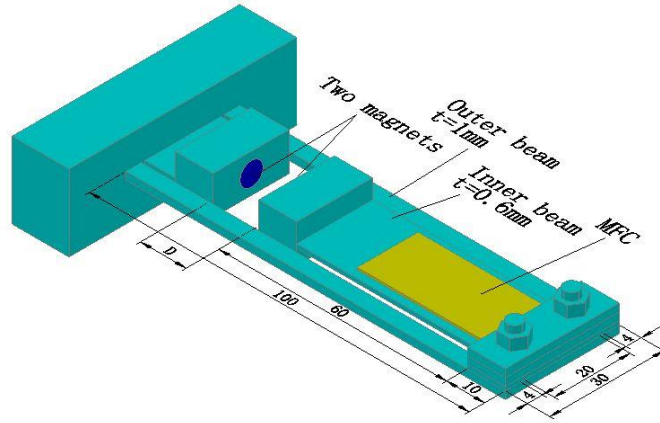
Figure 3. Illustration of nonlinear 2-DOF harvester (all dimensions in mm)

In the experimental parametric study, three parameters are adjusted to study the behavior of the system. They are: the distance of the two magnets (D), the tip mass of the outer beam (M_1), and the base excitation level (A). The distance of two magnets which affects the nonlinear stiffness of the system and the base excitation level are two key parameters determining the nonlinear dynamics of the harvester. Also, adjusting M_1 affects the nonlinear response patterns of various configurations. Different values of these three parameters used in the experiment are listed in Table 2.

Table 2. Values for parameters used in experiment study

Parameters	Values
Distance of two magnets, D (mm)	14, 12, 11, 10, 9
Tip mass at the end of outer beam, M_1 (g)	13.1, 11.2, 9.3, 7.4, 5.5, 3.6
Harmonic base excitation level, A (m/s^2, RMS)	0.5, 1, 2

If the distance between two magnets is smaller than certain value, due to the strong repulsive magnetic force, the structure will have two stable equilibrium positions (thus two potential wells). This is called bi-stable configuration, as illustrated in Figure 4. The central position is the stable equilibrium position in the mono-stable configuration, which however becomes the potential barrier in the bi-stable configuration. When the distance between two magnets decreases further, the two equilibrium positions will be separated further away from each other, and the central potential barrier will increase, making it harder to cross. Thus, the dynamics of the bi-stable configuration will be more complicated than that of mono-stable one. Small-amplitude oscillations confined in one potential well, large-amplitudes oscillation crossing two potential wells, or even be chaotic responses may present, depending on the base excitation level and the initial condition (Tang et al., 2012). In this study, we focus on the

performance of the harvester in mono-stable configuration, while the bi-stable configuration will be briefly illustrated to show the difference. For the prototype studied in our experiment, the critical distance D for transition from mono-stable configuration to bi-stable one is observed as between 10 and 9 mm.
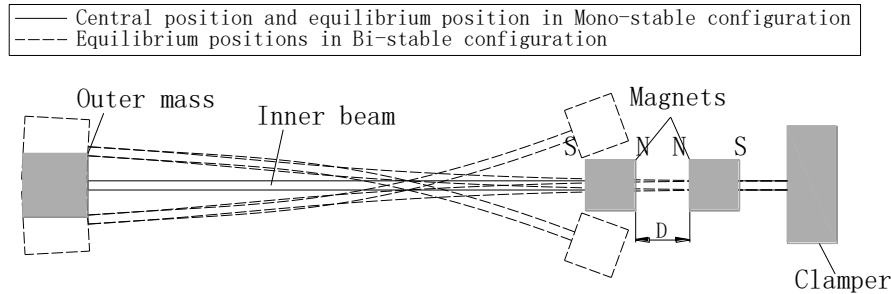

Figure 4. Illustration of equilibrium position for mono-stable and bi-stable vibrations

The harvester is firstly tested with sinusoidal sweep to obtain the frequency response curves for different configurations, from which an optimal configuration is determined. Subsequently, the optimal nonlinear 2-DOF harvester is tested under random excitation to compare its performance with that of the linear counterpart.

3.2 Frequency response for sinusoidal sweep

The acceleration for the base excitation is kept constant for every sinusoidal sweep. The frequency responses of open circuit voltage from the nonlinear 2-DOF energy harvester are recorded in terms of the root mean square (RMS) values as the harvester is vibrating in the steady state. At some unique frequencies, the transient responses are recorded as well. With various distances between the two magnets, linear response, quasi-linear response, mono-stable nonlinear response and bi-stable nonlinear response are observed, and an optimal configuration is concluded which can achieve significantly wider bandwidth.

Frequency response of linear 2-DOF harvester (without magnetic force)

By removing the magnet which clamped at the shaker, the system becomes a linear 2-DOF harvester. Its frequency responses, including three groups of experimental results with different mass values, are shown in Figure 5. It is observed that the first peak slightly changes due to different M_1 while the second peak is almost not affected. Here, the two natural frequencies (about 15 Hz and 28 Hz for case (a)) are still a bit far away from each other, and the magnitude of the first peak is relatively small

compared to the second. Thus, the linear harvester is not optimized to achieve two close response peaks with adequate magnitudes.
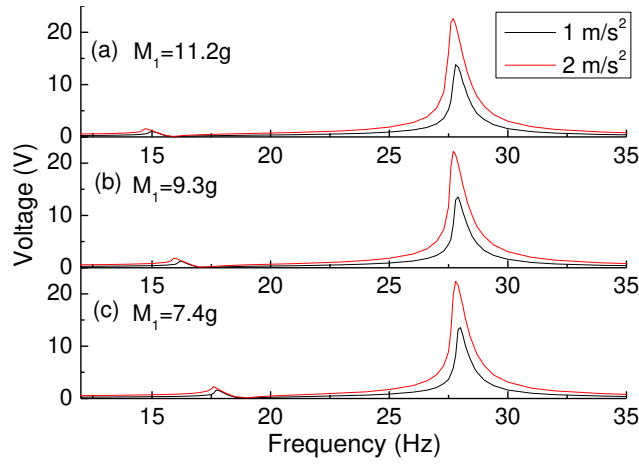

Figure 5. Frequency response of linear 2-DOF harvester, (a) M_1=11.2g, (b) M_1=9.3g, and (c) M_1=7.4g.

Quasi-linear response of nonlinear configuration with lower excitation level

When the 2-DOF harvester with nonlinear configuration is tested under low excitation level (0.5 m/s^2), it exhibits a quasi-linear behavior which is similar to the linear harvester (Figure 6). Under low excitations, the vibration amplitude of the structure is not significant, thus the linear component of the magnetic force dominates and changes the linear stiffness of the system (mostly affect the inner beam). It can be seen from Figure 5(a) and Figure 6, with different distances between the two magnets D, the resonant frequency for the second peak is tuned (from 28 Hz to 17.5 Hz) while the first resonant peak remains at the same position (around 15 Hz). Meanwhile, the magnitude of the first peak increases and the second peak decreases gradually with the decrease of the magnets distance. Moreover, an anti-resonance point can be clearly observed in front of the first peak (highlighted with red circle), which is very similar to the pattern of the inner beam in linear 2-DOF case (Group B in Table 1). It is important to note that the configuration in case (d) of Figure 6 meets the requirements for the design of a broadband energy harvester, which presents two close response peaks of adequate magnitudes with anti-resonance point outside the two peaks range. Under higher excitations, the bandwidth for such system can be further increased, which will be detailed in the following section. Besides, it should be mentioned that further decrease of the magnets distance (D) tunes the harvester into bi-stable configuration. As observed from Figure 6, when the distance between the magnets decreases, the amplitude of the second response peak slightly drops. Meanwhile, the amplitude of first peak, as well
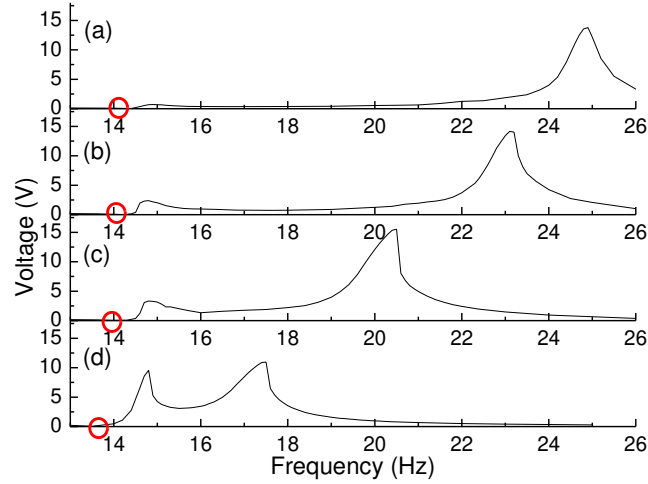
10

Figure 6. Quasi-linear frequency response for nonlinear 2-DOF harvester under base excitation of 0.5 m/s² with M_1=11.2 g and (a) D=14 mm, (b) D=12 mm, (c) D=11 mm (d) D=10 mm.

Mono-stable nonlinear response with higher excitation level

With two magnets placed closer for mono-stable configuration (D=10 mm), the response curve presents very minor hardening nonlinear behavior under low excitation, that is, the second peak is slightly bent to the higher frequency direction, as shown in Figure 7(a). However, the upward and downward sweeps do not have obvious difference, thus it still can be regarded as a quasi-linear response.

When the excitation level increases, the response curve, especially the second peak, is bent further to the higher frequency direction, providing enlargement in bandwidth, as shown in Figure 7(b) and (c). Also, the typical jump phenomenon and multi-valued response of mono-stable configurations are observed (i.e. from 18.5Hz to 20Hz in Figure 7(c), large-amplitude and small-amplitude oscillation orbits co-exist). If 10V is regarded as a useful working voltage level, the upward sweep ensures the harvester to capture the higher energy orbit and cover a bandwidth of about 5 Hz (15 Hz to 20 Hz). However, the higher voltage response obtained from the upward sweep cannot be always guaranteed in the practical application. By considering the downward sweep response curve, which is more robust for any initial condition, the bandwidth is still quite large of about 3.5 Hz (15 to 18.5 Hz).

As observed from Figure 7, the amplitudes of frequency responses do not increase proportionally to the excitation level, especially for the first peak. This may due to the geometric constraint that the vibration amplitude of the structure cannot increase infinitely with the excitation.
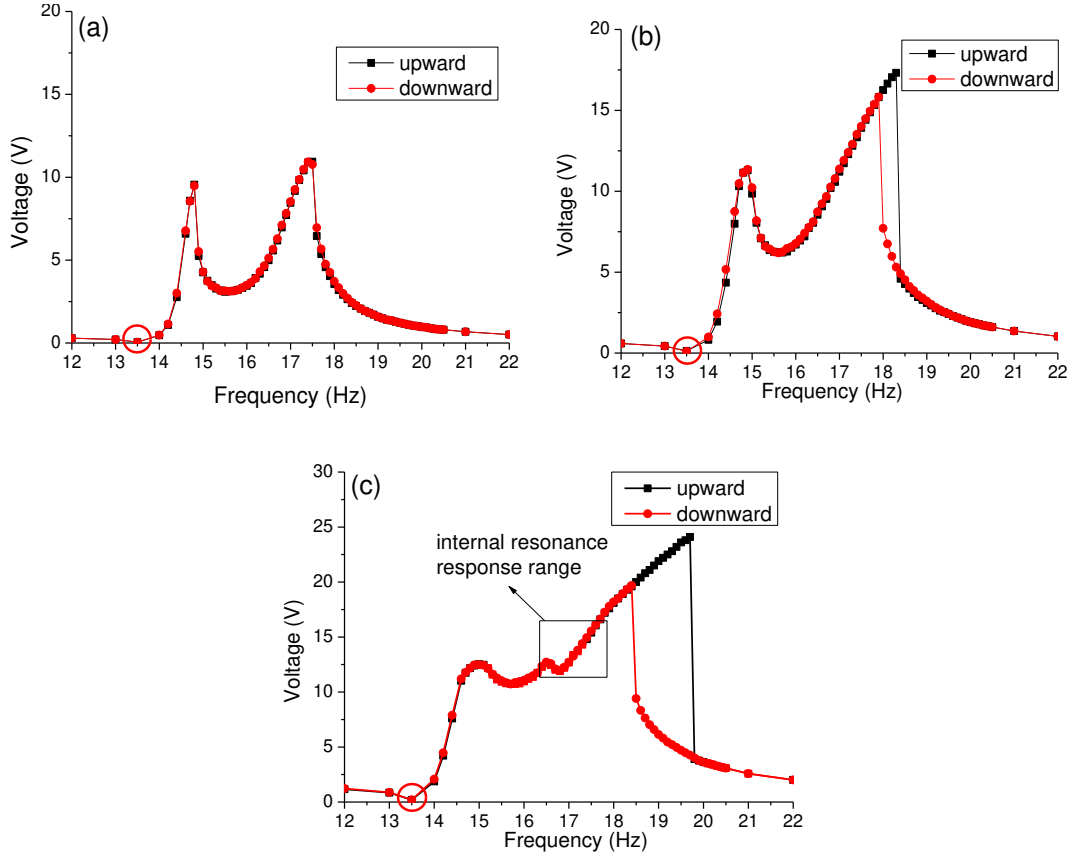

Figure 7. Frequency responses for nonlinear 2-DOF harvester with M_1=11.2g and D=10mm under excitation of (a) 0.5m/s^2 (b) 1m/s^2 and (c) 2m/s^2

Moreover, within certain frequency range (as indicated in Figure 7(c)), the response is not harmonic though the system is under harmonic excitation. Transient voltage responses for several frequency points are shown in Figure 8. It is clear in Figure 8 that any of the four waveforms can be viewed as a combination of several harmonic waveforms with different frequency. As observed in the experiment, the vibration motion of the harvester was constantly swapping between its two vibration modes, which can be regarded as the internal resonance for the nonlinear system. In Figure 7(c), an additional peak presents within such frequency range. Actually, the presence of this peak is due to the variation of the RMS value for those non-harmonic waveforms. As observed in the experiment, this phenomenon is more obvious when the excitation level is higher.
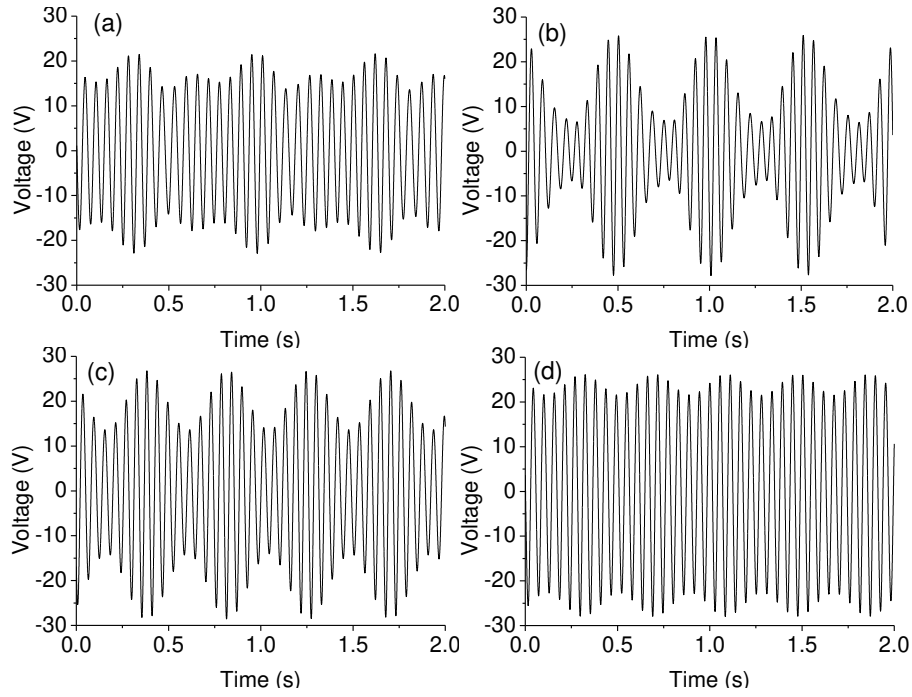
Figure 8. Transient voltage responses of nonlinear 2-DOF harvester at (a) 16.4Hz, (b) 16.9Hz, (c) 17.4Hz and (d) 17.8Hz

It is worth mentioning that the broadband performance of the nonlinear 2-DOF harvester is achieved by properly selecting the structural parameters (M_1=11.2g) and the distance between magnets (D=10mm). Similar to the linear 2-DOF harvester, we achieve two close peaks, both with adequate amplitudes, and the negative effect of anti-resonance for broadband performance is mitigated by avoiding its appearance in-between the peaks. Moreover, the nonlinearity introduced into the system further widens the bandwidth by bending the second peak and filling the valley between the peaks. But such broadband performance may be deteriorated with improperly selected parameters.

Figure 9 provides more cases of the linear 2-DOF harvester with different M_1. For case (a) in Figure 9, the anti-resonance point is located in-between the two response peaks, which is similar to the pattern of inner beam for Group C in Table 1. For cases (b) and (c), the two resonant frequencies are tuned close to each other, and the bandwidth is reduced as compared to Figure 7. On the contrary, for case (d), the two resonant frequencies are tuned too far away, making the output between two peaks deteriorated. Thus, considering the case in Figure 7 and the four cases in Figure 9, we conclude that the configuration of nonlinear 2-DOF harvester with M_1=11.2g and D=10mm is the optimal configuration for this mono-stable nonlinear 2-DOF harvester. Here, the optimal configuration refers to the best one which produces largest bandwidth with respectable amplitude, when the tip masses vary from 7.4 to

13
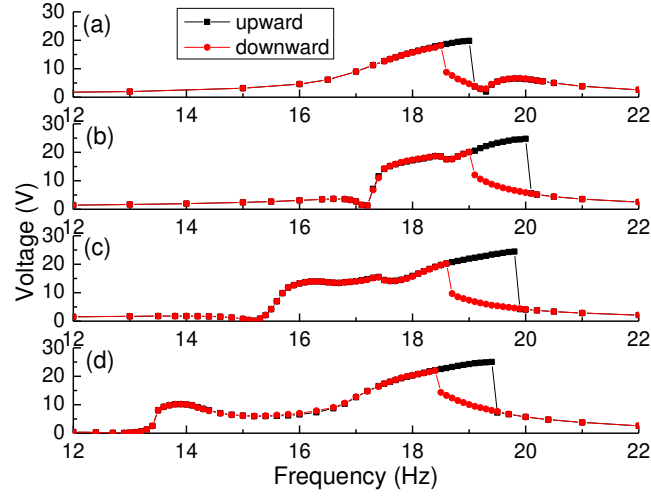
Figure 9. Frequency response for nonlinear 2-DOF harvester with D=10 mm, A=2m/s^2 and (a) M$_1$=5.5g, (b) M$_1$=7.4g, (c) M$_1$=9.3g and (d) M$_1$=13.1g.

When the distance between two magnets is further decreased (D≤9mm), the harvester will move into bi-stable configuration, which is more complicated than the mono-stable vibration. According to our experimental observation, the harvester was easily confined in one potential well due to the gravity and fabrication defect. The dynamics and frequency response will be much different from the mono-stable configuration. The investigation of the bi-stable configuration is beyond the scope of this paper.

In this work, the electromechanical coupling is quite low as K$_e^2$/ζ=0.2~0.3, (Ke is electromechanical coupling coefficient and ζ is mechanical damping ratio), which can be regarded as weak coupling condition (Shu and Lien, 2006). For weak electromechanical coupling, the frequency responses of the optimal power and open circuit voltage have very similar trends in spite of the slight resonant frequency shift. Thus, the frequency response of open circuit voltage can be used to study the bandwidth of the system and the conclusions in terms of open circuit voltage response apply to the harvested power as well.

3.3 Tests under random excitation

In real applications, the majority of vibration energy sources present in random patterns. In this section, the nonlinear 2-DOF harvester is tested under random excitation with a uniformly distributed acceleration spectrum from 8 Hz to 35 Hz, which covers all the frequency range for both linear and

nonlinear configurations developed in this work. In the experiment, a shaker controller (VR9500) is used to control the random vibrations of the shaker. Figure 10(a) shows an example of the controlled excitation spectrum for the experiment test, in which the demanded spectrum is a uniform distribution with RMS acceleration of 0.1G (gravitational acceleration). The time history of the acceleration of the base excitation from the shaker is also recorded, as shown in Figure 10(b). Three random excitation levels, 0.1G, 0.15G and 0.2G, are considered for random tests.
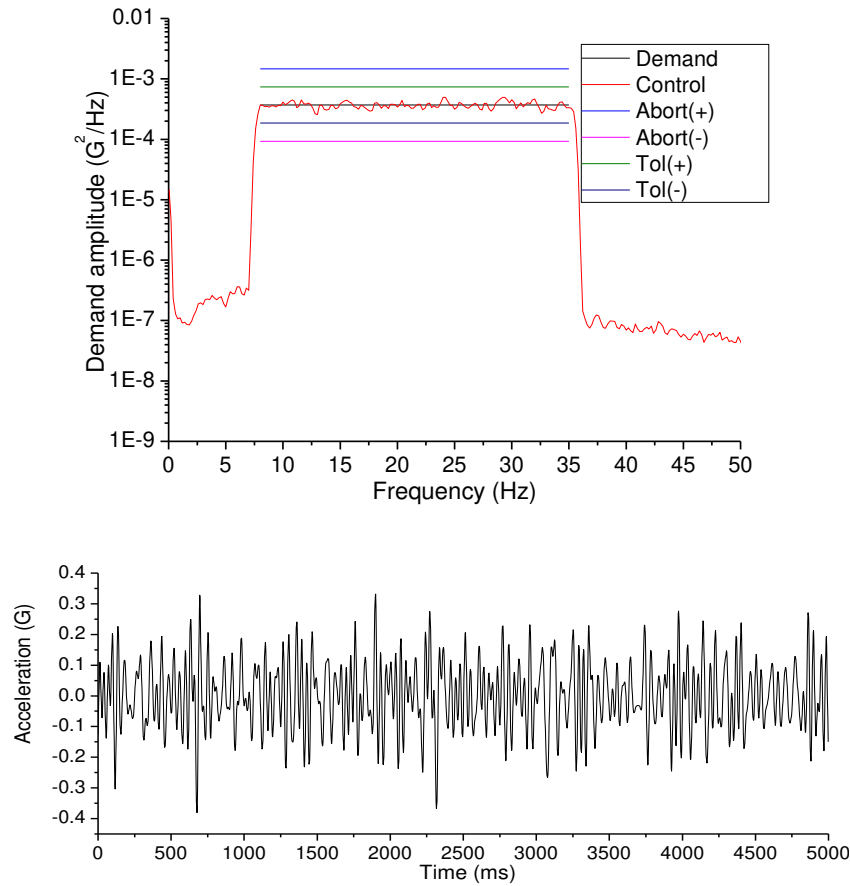

Figure 10. (a) Power density of demanded spectrum and controlled value for RMS acceleration=0.1 G,

(b) Time history of base excitation

The optimal 2-DOF nonlinear configuration (M_1=11.2g and D=10mm) obtained from the previous section is tested and evaluated under random excitation. Its performance will be compared with its linear counterpart (simply remove the clamped magnet).

Under the same level of random excitation, Figure 11 provides the examples of the waveforms of the open circuit voltage response for both the nonlinear and linear configurations. Obviously the magnitude of the response for the nonlinear 2-DOF harvester is much larger than its linear counterpart.

Power spectrums in the frequency domain are obtained by Fast Fourier Transformation (FFT), for both linear and nonlinear configurations, as shown in Figure 12. It can be observed that both the magnitude and the bandwidth are greatly improved for the nonlinear configuration compared to its linear counterpart.
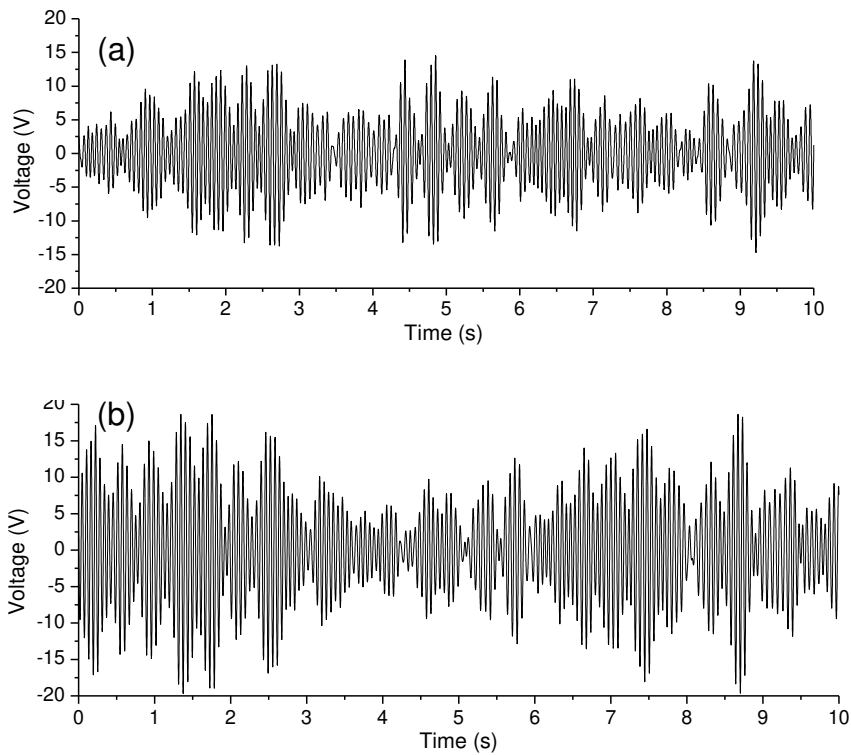

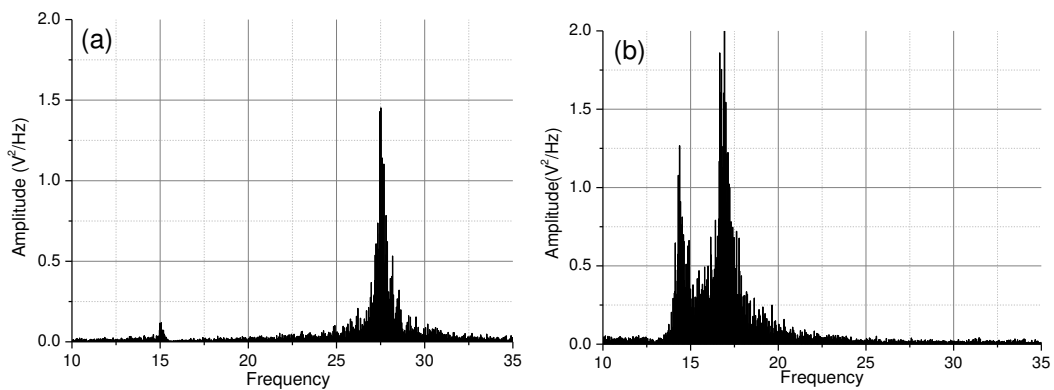Figure 11. Recorded waveforms under random excitation of RMS acceleration=0.1 G, (a) Linear, (b) Nonlinear

Figure 12. FFT result for recorded waveform, (a) Linear, (b) Nonlinear

To further evaluate the performance of the system, the harvester is connected with an energy storage circuit composed of an AC/DC full-wave rectifier and a storage capacitor (330μF). In the experiment, the charging procedure is carried out for 2 minutes each time, and the voltage at the capacitor is monitored to calculate how much energy can be accumulated, as shown in Figure 13. For each random excitation level, the same procedure is repeated for 4-5 times to ensure the reliability of the results.

From the comparison shown in Figure 13, the performance of the nonlinear harvester is much better than that of its linear counterpart. For all the tested cases, the accumulated energy in the capacitor ($E = 1/2CU^2$) by the nonlinear harvester is about 2.5 times larger than its linear counterpart. For example, the average energy stored for the nonlinear harvester with excitation of 0.2G is about 5.5 mJ, while the linear one only achieves about 2.2mJ. Other than this standard charging circuit, many other circuit techniques proposed by researchers, i.e. SSHI techniques (Liang and Liao, 2012), can be considered to further improve the power output of the developed nonlinear harvester.
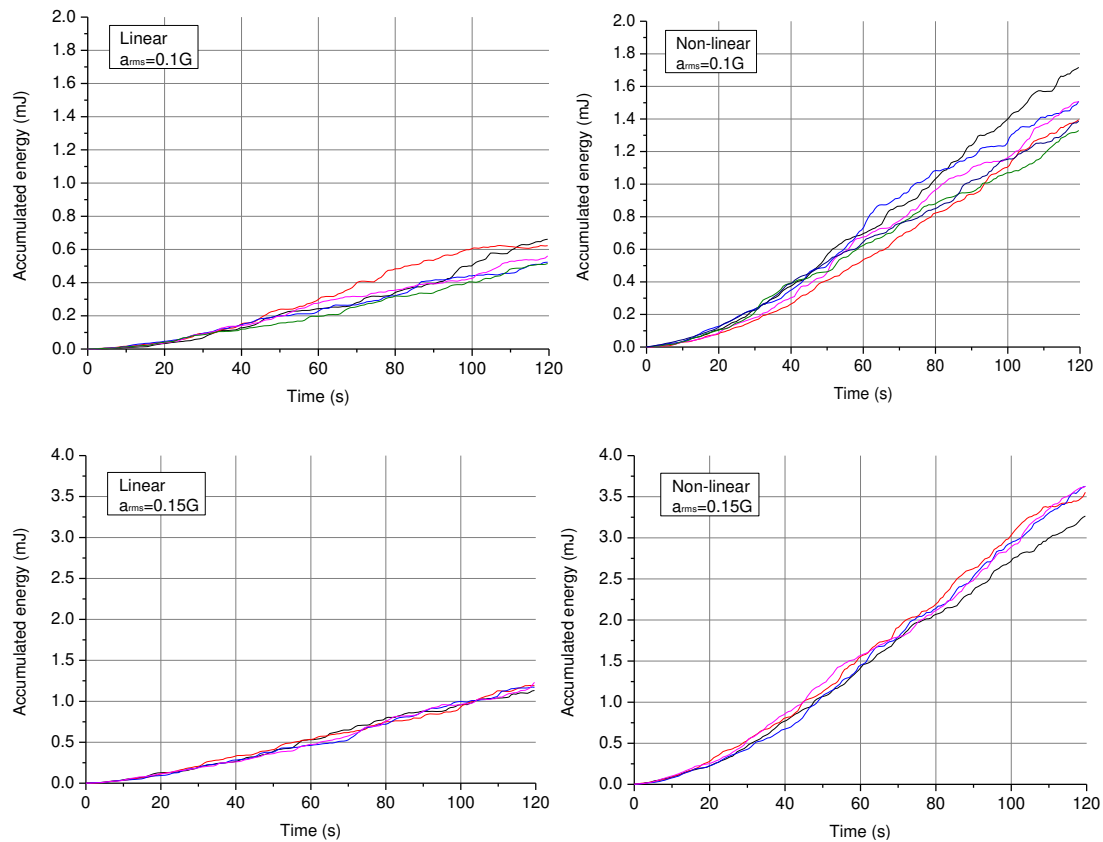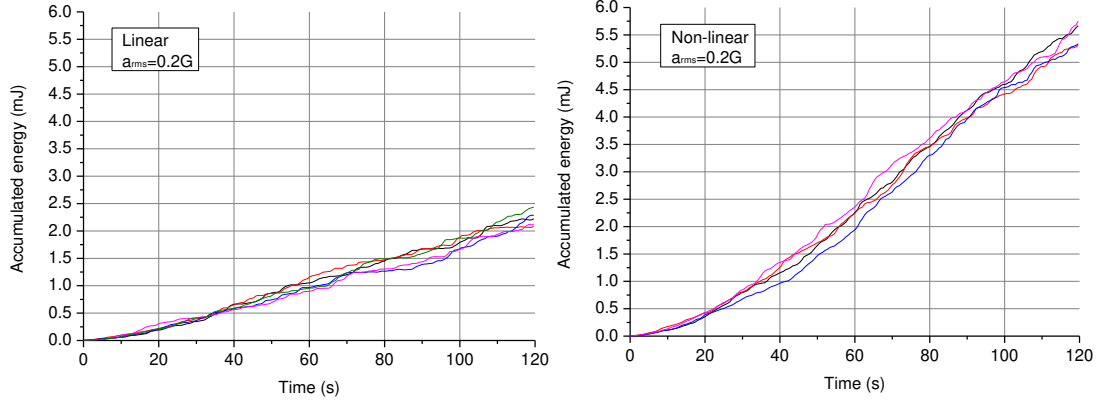
Figure 13. Charging record for nonlinear and linear 2-DOF harvester with different excitation levels

4. MODELING OF NONLINEAR 2-DOF HARVESTER AND VALIDATION

4.1 Modeling of linear 2-DOF harvester

In this section, a lumped parameter model for the nonlinear 2-DOF harvester is presented. The modeling results are obtained using numerical integration in Matlab and validated against the experiment outcome.

With the mass and stiffness matrices obtained in Equations (1) and (2), the vibration motion of the linear 2-DOF system subjected to base vibration can be described by

$$\begin{cases} M_1\ddot{x} + C_{11}\dot{x} + K_{11}x + C_{12}\dot{y} + K_{12}y = -M_1\ddot{u}_0 \\ M_2\ddot{y} + C_{12}\dot{x} + K_{21}x + C_{22}\dot{y} + K_{22}y = -M_2\ddot{u}_0 \end{cases} \tag{4}$$

where x and y are the displacements for outer mass and inner mass, respectively; $\ddot{u}_0$ is the base acceleration; and K_{ij} and C_{ij} denote the related components in the stiffness and damping matrices, respectively. When simplifying the harvester using the lumped-mass model, the mass values used in the equations should be modified with a correction factor, as the distributed mass of the cantilever will also contribute to the vibration motion (Erturk and Inman 2008). However, when the tip mass is much larger than the distributed mass of cantilever, the correction factor is very close to unity. For example, by considering the optimal configuration of our experiment, tip mass M1=11.2g and the distributed mass of outer beam is about 2.7g. The correction factor can be calculated as 1.03, by using the equations in Erturk and Inman (2008). Thus, for qualitative analysis using the lumped-mass model, the correction factor is not applied in this work.

The damping matrix is assumed to be proportional to the mass and stiffness matrices as

$$[C] = \mu[K] + \lambda[M] \tag{5}$$

where μ and λ are two coefficients. To determine these coefficients, an attenuation test for the experiment prototype is carried out to measure the damping ratio (ζ) at the first and second resonances. The measured damping ratio does not vary too much for different conditions, and the value is around 0.8% for both resonances. With known damping ratios at the resonant frequencies, the two coefficients as well as the damping matrix are then obtained.

With the piezoelectric transducer attached on the inner beam, an electrical-mechanical coupling equation is required to relate the vibration motion with the electrical output. However, in this 2-DOF cantilever harvester, the strain is not simply related to the displacements 'x' and 'y'. The angle of rotation at the tip mass is also related to the strain in the beam. Figure 14 illustrated the displacements and angle of rotation in stationary condition, where the dashed line of the inner beam indicates the "free position" that no strain occurs in it.
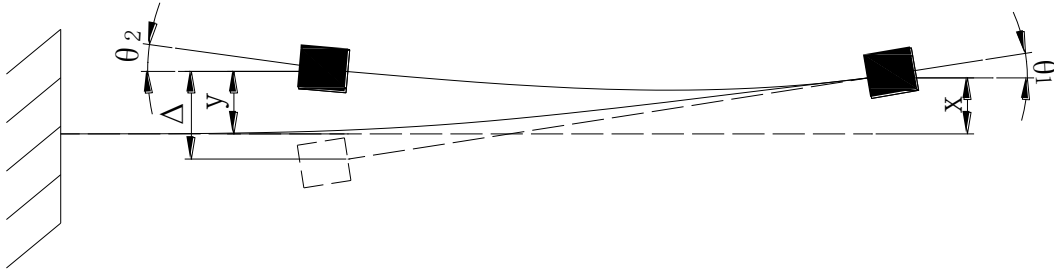
Figure 14. Stationary displacement and angle rotation relation

The strain distribution in the inner beam should be proportional to the overall displacement from the "free position" to the forced position, which is indicated as "Δ" in Figure 14. To obtain Δ, the angle of rotation at the outer mass should be obtained first, which is expressed as

$$\theta_1 = \varphi_{11}(K_{11}x + K_{21}y) + \varphi_{21}(K_{12}x + K_{22}y) \tag{6}$$

where φ_{ij} denotes the angle of rotation at position j when a unit force is applied at position i.

$$\varphi_{11} = \frac{L_1^2}{2EI_1}$$

$$\tag{7}$$

$$\varphi_{21} = \frac{(L_1 - L_2)^2 - L_2^2}{2EI_1}$$

Finally the overall displacement Δ is

$$\Delta = y - x + \theta_1 L_2 = \alpha y - \beta x \tag{8}$$

$$\alpha = 1 + (\varphi_{11}K_{21} + \varphi_{21}K_{22})L_2$$

$$\beta = 1 - (\varphi_{11}K_{11} + \varphi_{21}K_{12})L_2$$

Therefore, the coupled governing equation of the 2-DOF system should be written as,

$$\begin{cases} M_1\ddot{x} + C_{11}\dot{x} + K_{11}x + C_{12}\dot{y} + K_{12}y - \psi V = -M_1\ddot{u}_0 \\ M_2\ddot{y} + C_{12}\dot{x} + K_{21}x + K_{22}y + C_{22}\dot{y} + \psi V = -M_2\ddot{u}_0 \\ \qquad -\psi(\dot{\Delta}) + C_s\dot{V} + V/R = 0 \end{cases} \tag{9}$$

where ψ is an electrical-mechanical coupling coefficient related to the property of piezoelectric material and the vibration modal shape; C_s is the capacitance of the piezoelectric element; R is the electric load connected to the harvester; and V is the voltage cross the load. In this model, ψ is equal to 9.2e-5 NV^{-1} and C_s is 25 nF. To emulate the open circuit condition, R is set to be 1000MΩ.

4.2 Dipole-dipole magnetic interaction

In the proposed 2-DOF nonlinear harvester, the magnetic force is simplified as a dipole-dipole magnetic interaction. In vector form, its general expression is (Levitt and Malcolm, 2001),

$$\vec{F}_{mag} = \frac{3\mu_0 m_a m_b}{4\pi|r|^4} [\hat{r} \times \hat{m}_a \times \hat{m}_b + \hat{r} \times \hat{m}_b \times \hat{m}_a - 2\hat{r}(\hat{m}_a \cdot \hat{m}_b) + 5\hat{r}(\hat{r} \times \hat{m}_a) \cdot (\hat{r} \times \hat{m}_b)] \tag{10}$$

where μ_0 is the permeability of space (4πe^{-7} Tm/A); m_a and m_b are the magnetic moment for the two magnets (in the experiment, $m_a = m_b = 0.218$Am^2); r is the distance of two magnetic dipoles; $\hat{r}, \hat{m}_a, \hat{m}_b, \hat{\jmath}$ and $\hat{k}$ are the units vector with directions shown in Figure 15. In this nonlinear 2-DOF harvester, one magnet is fixed at the shaker thus its position and orientation does not change, while the other is attached at the tip of the inner beam with displacement and angle of rotation during vibration.

By applying these restrictions into Equation 10, the magnetic force can be expressed as

$$\vec{F}_{mag} = \frac{3\mu_0 m_a m_b}{4\pi|r|^4} [\hat{k} \sin(a) + \hat{\jmath} \sin(a+b) + 2\hat{r} \cos(b) - 5\hat{r} \sin(a) \sin(a+b)] \tag{11}$$

The angles a and b in Figure 15 are also related to the displacements of the outer mass (x) and inner mass (y).

$$a = \arctan(\frac{y}{D\prime}) \tag{12}$$

$$b = \theta_2 = \varphi_{12}(K_{11}x + K_{21}y) + \varphi_{22}(K_{12}x + K_{22}y) \tag{13}$$

Finally the magnetic force in the vertical direction is obtained as

$$F_{mag_v} = \vec{F}_{mag} \cdot \hat{j}$$

$$= \frac{3\mu_0 m_a m_b}{4\pi |r|^4} [\sin(a)\cos(b) + \sin(a+b) + 2\cos(b)\sin(a) - 5\hat{r}\sin(a)\sin(a+b)]\sin(a) \quad (14)$$
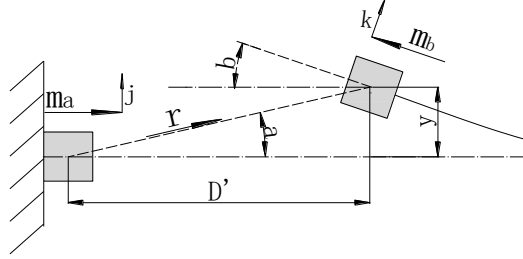

Figure 15. Relative position inner mass

It should be noted that, in the experiment, the distance D between the magnets is measured from the facing surfaces of the two magnets. While, in the modeling with the assumption of dipole-dipole magnetic interaction, the horizontal distance D' is calculated from centre to centre of the magnets, i.e., D'=D+5, as the thickness of the two cylinder magnets are both 5 mm.

By adding this magnetic force into Equation (9), the governing equation of the nonlinear 2-DOF system is obtained as

$$\begin{cases} M_1\ddot{x} + C_{11}\dot{x} + K_{11}x + C_{12}\dot{y} + K_{12}y - \psi V = -M_1\ddot{u}_0 \\ M_2\ddot{y} + C_{12}\dot{x} + K_{21}x + K_{22}y + C_{22}\dot{y} + \psi V + F_{mag\_v} = -M_2\ddot{u}_0 \\ -\psi(\alpha\dot{y} - \beta\dot{x}) + C_s\dot{V} + V/R = 0 \end{cases} \quad (15)$$

For simplicity, only the vertical component of the magnetic force is considered in Equation 14, while the horizontal component is neglected. Note that, the magnetic force is only applied to the inner mass. This is why in the experiment the nonlinearity mostly affects the second response peak which is dominated by the inner beam.

4.3 Numerical computations and results

Since it is very difficult to solve Equation (15) including nonlinear term analytically, we resort to numerical integration techniques using Runge-Kutta method (which are readily available in Matlab) to obtain the numerical results. By numerically solving the ordinary differential equation with given initial conditions, the steady-state vibration waveform can be obtained for every frequency point. Thus the response curve for the frequency sweep can be plotted. All structural parameters are set according to the experiment setup, as shown in Figure 3, and the optimal configuration is chosen to be validated. Other parameters used for numerical computation are listed in the following Table (3).

Parameters	Values
Outer effective mass, M_1 (g)	11.8
Inner effective mass, M_2 (g)	7.9
Damping ratio, ζ	0.8%
Stiffness matrix, K (N/m)	$\begin{bmatrix} 138.5 & 10.4 \\ 10.4 & 207.4 \end{bmatrix}$
Damping matrix, C (10^{-3} N·sec/m)	$\begin{bmatrix} 27.31 & 1.22 \\ 1.22 & 31.46 \end{bmatrix}$
Magnetic moment, m_a & m_b (Am^2)	0.218
Permeability of space, μ_0 (Tm/A)	$4\pi e^{-7}$
Electromechanical coupling coefficient, ψ (N/V)	9.2e-5
Capacitance of the piezoelectric element, C_s (nF)	25
Electric load resistor, R (Ω)	1e9

Figure 16 shows simulation results under low excitation level of 0.5m/s^2, to illustrate the trend of the resonance tuning by adjusting the value of the distance between two magnets, which is similar to the experiment results in Figure 6 except for slight differences in the peak locations and amplitudes. The value of the distance between two magnets does not exactly match with the experiment to achieve the optimal configuration.
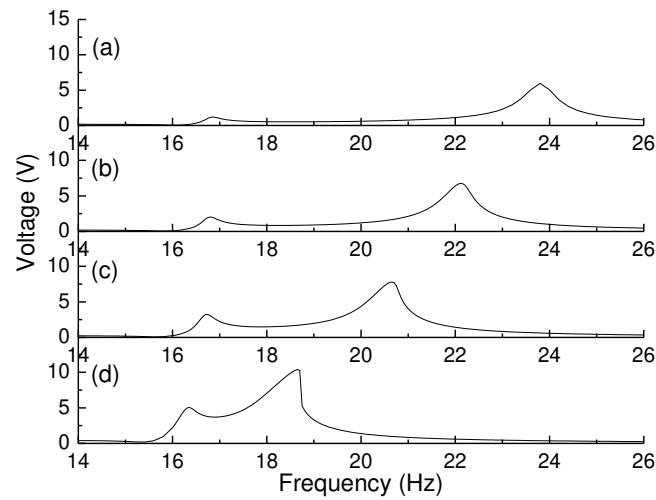

Figure 16. Voltage response for optimal configuration under low excitation level of 0.5 m/s^2 and with

(a) D'=18 mm, (b) D'=16 mm, (c) D'=15 mm (d) D'=14 mm

Figure 17 shows the theoretical results for different base excitation levels, which is similar to the experiment results shown in Figure 7, however the peak locations and amplitudes does not exactly match. It is also observed the existence of an anti-resonance point in front of the first response peak. Moreover, as shown in Figure 17(c), there is a fluctuation of the frequency response curve around 18

Hz, which indicates the occurrence of the internal resonance. The transient voltage waveform for the frequency of 18.3 Hz is recorded in Figure 17, which shows the similar phenomenon observed in the experiment.
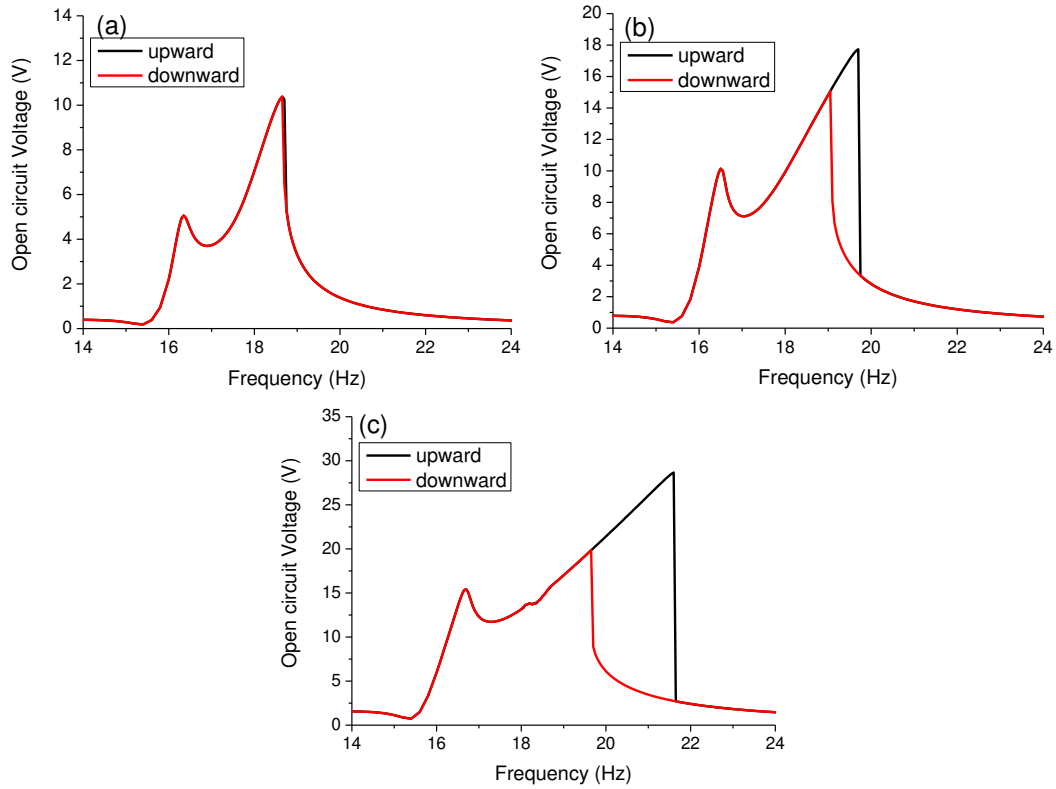

Figure 17. Voltage response for optimal configuration with D'=14mm under (a) 0.5 m/s^2 (b) 1 m/s^2 and
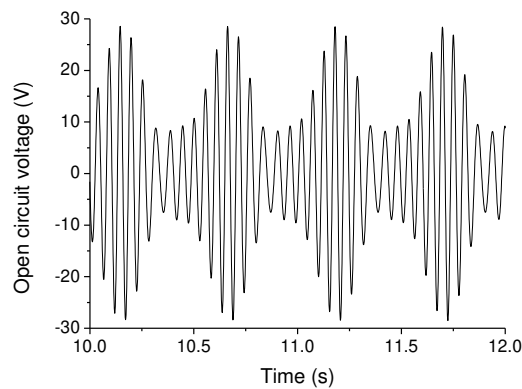
(c) 2 m/s^2

Figure 19. Waveform of the voltage response at 18.3 Hz

In summary, the results from the lumped parameter model indicate similar trend in the frequency response of the nonlinear harvester. The internal resonance is captured as well in the modeling results.

The results from the lumped parameter modeling validates that this nonlinear 2-DOF harvester can achieve broader operation bandwidth with proper chosen parameters. Although discrepancies exist between the theoretical modeling and the experimental results, the model predicts similar trend regarding the peak change and nonlinear vibration phenomenon to the experiment. Therefore, it can be used as a tool for parametric study of resonances and bandwidth tuning, which would provide initial estimate for the parameters in the optimal configuration. When doing so, the parameters should be chosen such that (1) no anti-resonance exists in the desired frequency range (e.g. choose the parameters that produce the inner beam response in Group B of Table 1); and (2) two response peaks are close with significant output.

5. CONCLUTIONS

A new nonlinear 2-DOF piezoelectric energy harvester is proposed to combine the multi-modal energy harvesting with the nonlinear vibration technique, and evaluated by the experimental parametric study. By properly choosing the structural parameters and the distance between the magnets, the two resonant response peaks can be tuned to be close enough and both with adequate amplitude. Meanwhile, the negative effect of the anti-resonance for broadband energy harvesting can be mitigated by avoiding its appearance in-between two peaks. The nonlinearity helps further broaden the useful bandwidth. Based on the experimental parametric study of the nonlinear 2-DOF harvester, an optimal configuration is determined, which provides much broader bandwidth and much higher efficiency when charging a storage capacitor compared to its 2-DOF linear counterpart. A lumped parameter model of the 2-DOF nonlinear harvester is also developed considering the dipole-dipole magnetic force. This model successfully predicts the similar broadband response trend of the proposed harvester as experiment.

REFERENCES

Challa V.R., Prasad M.G., Shi Y. and Fisher F.T., 2008, "A Vibration Energy Harvesting Device with Bidirectional Resonance Frequency Tunability," *Smart Materials and Structures* 17, 015035.

Cottone F., Vocca H. and Gammaitoni L., 2009, "Nonlinear Energy Harvesting," *Physics Review Letters*, 102, 080601.

Erturk A., and Inman D.J., 2008, "On Mechanical Modeling of Cantilevered Piezoelectric Vibration Energy Harvesters," *Journal of Intelligent Material Systems and Structures*, 19, 1311-1325.

Erturk A., Hoffmann J. and Inman D.J., 2009a, "A Piezomagnetoelastic Structure for Broadband Vibration Energy Harvesting," *Applied Physics Letters*, 94, 254102.

Erturk A., Renno J.M. and Inman D.J., 2009b, "Modeling of Piezoelectric Energy Harvesting from an L-Shaped Beam-Mass Structure with an Application to UAVs," *Journal of Intelligent Material Systems and Structures*, 20, 529-544.

Ferrari M., Ferrari V., Guizzetti M., Marioli D. and Taroni A., 2008, "Piezoelectric Multifrequency Energy Converter for Power Harvesting in Autonomous Microsystems," *Sensors and Actuators A*, 142, 329-335.

Jang S.-J, Rustighi E, Brennan M.J., Lee, Y.P. and Jung, H.-J., 2011, "Design of A 2dof Vibrational Energy Harvesting Device," *Journal of Intelligent Material Systems and Structures,* 22: 443–448.

Kim I.-H., Jung H.-J., Lee B.M. and Jang S.-J., 2011, "Broadband Energy-Harvesting Using A Two Degree-of-Freedom Vibrating Body," *Applied Physics Letters,* 98, 214102.

Meirovitch L. 2003, "*Fundamentals of Vibrations"*, New York, McGraw-Hill

Levitt and Malcolm H., 2001, "*Spin dynamics: basics of nuclear magnetic resonance*", Chichester: John Wiley & Sons.

Liang J.R. and Liao W.H., 2012, "Improved Design and Analysis of Self-Powered Synchronized Switch Interface Circuit for Piezoelectric Energy Harvesting Systems," *IEEE Transactions on Industrial Electronics*, 59, 1950-1960.

Lien, I.C. and Shu, Y.C., 2012, "Array of Piezoelectric Energy Harvesting by the Equivalent Impedance Approach," *Smart Materials and Structures*, 21, 082001.

Ou, Q., Chen, X., Gutschmidt, S., Wood, A., Leigh, N. and Arrieta, A. F., 2012 "An experimentally validated double-mass piezoelectric cantilever model for broadband vibration-based energy harvesting," *Journal of Intelligent Material Systems and Structures,* 23, 117-126.

Shahruz S.M., 2006, "Design of Mechanical Band-pass Filters for Energy Scavenging," *Journal of Sound and Vibration*, 292, 987-998

Shu Y. C. and Lien I. C., 2006, "Efficiency of energy conversion for a piezoelectric power harvesting system" *Journal of Micromechanics and Microengineering*, 16, 2429

Stanton S. C., McGehee C. C. and Mann B. P., 2009, "Reversible Hysteresis for Broadband Magnetopiezoelastic Energy Harvesting," *Applied Physics Letters*, 95, 174103.

Tadesse Y., Zhang S. and Priya S., 2009, "Multimodal Energy Harvesting System, Piezoelectric and Electromagnetic," *Journal of Intelligent Material Systems and Structures,* 20, 625-632.

Tang L.H. and Yang Y.W., 2012, "A Multiple-Degree-of-Freedom Piezoelectric Energy Harvesting Model," *Journal of Intelligent Material Systems and Structures*, 23, 1631-1647.

Tang, L.H., Yang Y.W. and Soh C.K., 2013, "Broadband Vibration Energy Harvesting Techniques," In *Advances in Energy Harvesting Methods*, pp.17-61. Springer New York.

Tang L.H., Yang Y.W. and Soh C.K., 2012, "Improving functionality of vibration energy harvesters using magnets," *Journal of Intelligent Material Systems and Structures*, 23, 1433-1449.

Wu H., Tang L.H. Yang Y.W. and Soh C. K., 2013, "A Novel Two-Degrees-of-Freedom Piezoelectric Energy Harvester," *Journal of Intelligent Material Systems and Structures*, 24, 357-368.